Application of admittance spectroscopy to evaluate carrier mobility in organic charge transport materials

S. W. Tsang and S. K. So[a)]
Department of Physics and Centre for Advanced Luminescence Materials, Hong Kong Baptist University, Kowloon Tong, Hong Kong, China

J. B. Xu
Department of Electronic Engineering, The Chinese University of Hong Kong, Shatin, Hong Kong, China

(Received 21 June 2005; accepted 18 November 2005; published online 10 January 2006)

We examine the feasibility of admittance spectroscopy (AS) and susceptance analysis in the determination of the charge-carrier mobility in an organic material. The complex admittance of the material is analyzed as a function of frequency in AS. We found that the susceptance, which is the imaginary part of the complex admittance, is related to the carrier transport properties of the materials. A plot of the computer-simulated negative differential susceptance versus frequency yields a maximum at a frequency τ_r^{-1}. The position of the maximum τ_r^{-1} is related to the average carrier transit time τ_{dc} by $\tau_{dc}=0.56\tau_r$. Thus, knowledge of τ_r can be used to determine the carrier mobility in the material. Devices with the structure ITO/4,4′,4″ -tris[*N*, -(3-methylphenyl)-*N*-phenylamino] triphenylamine/Ag have been designed to investigate the validity of the susceptance analysis in the hole mobility determination. The hole mobilities were measured both as functions of the electric field and the temperature. The hole mobility data extracted by susceptance analysis were in excellent agreement with those independently obtained from time-of-flight (TOF) measurements. Using the temperature dependence results, we further analyzed the mobility data by the Gaussian disorder model (GDM). The GDM disorder parameters are also in good agreement with those determined from TOF. © *2006 American Institute of Physics*. [DOI: 10.1063/1.2158494]

07 January 2026 12:25:54

I. INTRODUCTION

The discovery of high efficiency organic light-emitting diodes (OLEDs) in 1980s has triggered extensive research on organic semiconductors and devices.[1] The OLED is now a recognized contender for flat-panel displays. Besides OLEDs, organic field-effect transistors, and organic photovoltaic cells are showing very promising performances.[2–5] These developments depend on the accumulation of knowledge of the intrinsic properties of organic materials and related interfaces. Among them, charge-carrier transport and carrier injection are two key factors that govern the performance of a device.[6] With more understanding on the nature of carrier mobility in different organic materials, chemists are able to synthesize materials with desirable properties, and physicists or engineers can optimize device performance.

Time-of-flight (TOF) technique has been widely used to extract carrier mobility of organic materials.[7] TOF gives the bulk transport property of an organic film independent of the electrical contact at the metal/organic interface. However, due to the finite penetration depth of the incident laser, the technique generally requires a thick (>1 μm) film in order to have a well-defined flight distance. This requirement becomes an obstacle for characterizing new materials that are available in small quantities. Other techniques, such as dark-injection space-charge-limited current (DISCLC) transient, and transient electroluminescence can also be employed to extract the carrier mobility. Recently, admittance spectroscopy (AS) based on small signal space-charge-limited current (SCLC) theory has been proposed to characterize the carrier dynamics in organic materials.[8–10]

In this report, we provide an in-depth analysis of the complex admittance that describes the carrier dynamics inside an organic film sandwiched by two electrodes. It is found that the average transit time τ_{dc} of the carriers can be extracted from a plot of the negative differential susceptance $-\Delta B=-\omega(C-C_{geo})$ against the frequency $f=\omega/2\pi$, where C and C_{geo} are, respectively, the frequency dependent and geometric capacitances of the organic film. We show that τ_r^{-1}, the position at which the maximum in $-\Delta B$ plot occurs, is related to τ_{dc} by $\tau_{dc}=0.56\tau_r$. To verify this experimentally, we apply AS to characterize the hole-transporting properties of 4,4′,4″ -tris[*N*, -(3-methylphenyl)-*N*-phenylamino] triphenylamine (*m*-MTDATA). AS is then used to extract the hole mobility in *m*-MTDATA. In addition, we show that the disorder parameters in the Gaussian disorder model (GDM) extracted by AS are in excellent agreement with those measured independently by TOF.

II. THEORETICAL MODELING

We consider a two-terminal device consisting of an organic semiconductor with a dielectric constant ε and a thickness d, sandwiched between two electrodes. One of the electrodes (anode) is assumed to form an Ohmic contact with the organic material. The other contact is an electron blocking. Under a forward dc bias voltage of V_{dc}, holes are injected from the anode. After injection, holes are drifted towards the cathode. Given a fixed V_{dc}, we want to investigate analyti-

[a)]Author to whom correspondence should be addressed; electronic mail: skso@hkbu.edu.hk

 © 2006 American Institute of Physics

cally how the superposition of a small ac signal (modulation), with a frequency $f=\omega/2\pi$, affects the frequency-dependent complex admittance $Y(\omega)=G+i\omega C$, where $i^2=-1$ and G and C are, respectively, the conductance and the capacitance of the device.

The time (t)- and position (x)-dependent hole density $\rho(x,t)$ is given by the Poisson equation,

$$(\varepsilon/q)\frac{\partial E(x,t)}{\partial x}=\rho(x,t). \tag{1}$$

In Eq. (1), $E(x,t)$ is the time- and position-dependent electric field inside the organic material, and q is the charge of electron. The total current density $J(t)$ is given by

$$J(t)=q\rho(x,t)\mu(t)E(x,t)+\varepsilon\frac{\partial E(x,t)}{\partial t}. \tag{2}$$

For simplicity, the hole mobility μ in Eq. (2) is treated as field independent under small ac perturbation. However, in order to take into account the effect of dispersive transport, μ is considered to be time dependent.

In the Appendix, we write the electric field, charge density, and current density as sums of their dc and small signal ac components,

$$E(x,t)=E_{\mathrm{dc}}(x)+e(x,t),$$
$$\rho(x,t)=\rho_{\mathrm{dc}}(x)+\vartheta(x,t), \tag{3}$$
$$J(t)=J_{\mathrm{dc}}+j(t).$$

We show that, to the first order, the ac current density $j(t)$ can be written in the form

$$j(t)=q\mu(t)\rho_{\mathrm{dc}}(x)e(x,t)+\varepsilon\mu(t)E_{\mathrm{dc}}(x)\frac{\partial e(x,t)}{\partial x}+\varepsilon\frac{\partial e(x,t)}{\partial t}. \tag{4}$$

There are three contributions to $j(t)$. The first term in Eq. (4) describes the response of the dc charge-carrier density in the device. The second term gives the current due to the additional time-dependent injected charge-carrier density. The last term is due to the displacement current by charge relaxation. Since the admittance $Y=i_{\mathrm{ac}}/\nu_{\mathrm{ac}}$, the ac electric field in Eq. (4) can be solved by Fourier transform, giving

$$Y(\Omega)=\frac{\varepsilon A}{\tau_{\mathrm{dc}}d}\left(\frac{\Omega^3}{2i[0.75\tilde{\mu}(\Omega)]^2\{1-\exp[-i4\Omega/3\tilde{\mu}(\Omega)]\}+1.5\tilde{\mu}(\Omega)\Omega-i\Omega^2}\right). \tag{5}$$

In Eq. (5), A is the active area of the device. The normalized frequency is defined by $\Omega=2\pi f\tau_{\mathrm{dc}}=\omega\tau_{\mathrm{dc}}$. The normalized mobility is defined by $\tilde{\mu}(\Omega)=\mu(\Omega)/\mu_{\mathrm{dc}}$ where μ_{dc} is the dc mobility in the absence of the ac field. The details of calculation are given in the Appendix. The term inside the parenthesis is dimensionless and it describes how the transport properties of the organic material affect the complex admittance. To model the transport properties of a disordered organic material, we follow the approach adopted in Refs. 8, 9, and 11. We write the normalized mobility in the form

$$\tilde{\mu}(\Omega)=\mu(\Omega)/\mu_{\mathrm{dc}}=1+M(i\Omega)^{1-\alpha}, \tag{6}$$

where M and α are the dispersion parameters. For nondispersive transport, $\alpha=1$ and $M=0$. From Eqs. (5) and (6), and the fact that $Y\equiv G+iB=G+i\omega C$, one can simulate the frequency-dependent conductance G and capacitance C, using the three material-dependent parameters $\mu_{\mathrm{dc}}(=d^2/\tau_{\mathrm{dc}}V_{\mathrm{dc}})$, M, and α.

Figure 1 shows the results of simulation for G (top) and C (bottom) under different values of V_{dc} and dispersive parameters. For $V_{\mathrm{dc}}=0$ V, the capacitance is frequency independent and is equal to the geometrical capacitance $C_{\mathrm{geo}}=\varepsilon A/d$. However, the device capacitance exhibits significant frequency dependence when V_{dc} is positive (e.g., $V_{\mathrm{dc}}=1$ V). At high frequency (i.e., $\Omega>1$), $C=C_{\mathrm{geo}}$. When the probing frequency is smaller than τ_{dc}^{-1} (i.e., $\Omega<1$), the injected current lags behind ν_{ac} and therefore reduces the phase of Y. As a result, there is an inductive contribution to C, and C exhibits a minimum. At still lower frequency, there is a rapid in-

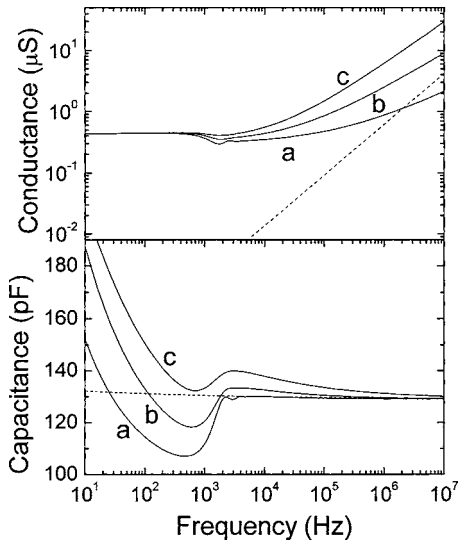

FIG. 1. Simulated frequency-dependent conductance (upper panel) and capacitance (lower panel) for an organic material with $\varepsilon_r=3$ and $\mu_{\mathrm{dc}}=10^{-5}$ cm^2 V^{-1} s^{-1}. The device is assumed to have an area $A=0.036$ cm^2 and a thickness $d=735$ nm under a dc bias of $V_{\mathrm{dc}}=1$ V. The dashed line indicates the case for $V_{\mathrm{dc}}=0$ V. Curves (a), (b), and (c) represent the different degrees of dispersion: (a) $M=0.05$ and $\alpha=0.5$ for less dispersive transport, (b) $M=0.10$ and $\alpha=0.4$ for dispersive transport, and (c) $M=0.15$ and $\alpha=0.3$ for highly dispersive transport.

07 January 2026 12:25:54

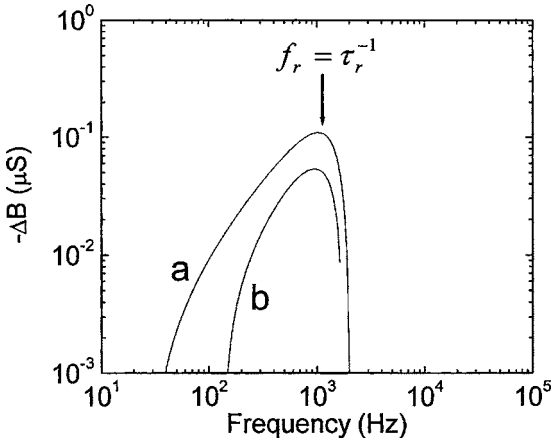

FIG. 2. Simulated $-\Delta B$ vs f plots obtained from Fig. 1(b). The positions of the maxima of curves (a) and (b) correspond to the relaxation time $\tau_r = 1/f_r$.

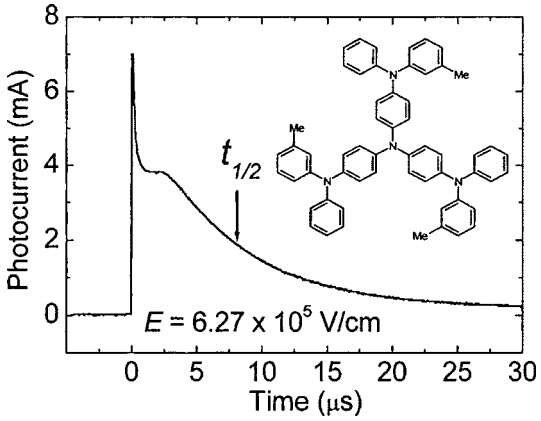

FIG. 3. A typical hole TOF transient at 289 K. The sample had a structure ITO/m-MTDATA (3.5 μm)/Al. The applied field was $E=6.27\times10^5$ V/cm. The average hole transit time τ_{dc} can be estimated from the TOF transient as the time $t_{1/2}$, that the current dropped to half of its value in the plateau region. The inset shows the chemical structure of m-MTDATA.

crease in C due to dispersive transport behavior, as indicated in the bottom panel of Fig. 1, curves (a), (b), and (c).

From the application point of view, AS will be particularly useful if the carrier mobility μ_{dc} (or transit time τ_{dc}) can be accurately and conveniently extracted from admittance measurements. References 12 and 13 reported that it is useful to plot the negative differential susceptance $-\Delta B=-\omega(C-C_{geo})$ in the frequency domain. This plot typically yields a maximum in $-\Delta B$ at a distinct frequency $f_r=\tau_r^{-1}$. Examples of simulated $-\Delta B$ vs f plots are shown in Fig. 2. In Ref. 12, it was argued that the position of the maximum in $-\Delta B$ plot should be related to the average carrier transit time τ_{dc}, and yet no clear relation was given. In order to clarify the relationship between τ_r and τ_{dc}, we performed computer simulation for $-\Delta B$ over a wide range of dispersion parameters α, M, and μ_{dc}. Our results show that $\tau_{dc}=0.56\tau_r$, for nondispersive transport. When the transport is dispersive, the scaling factor of 0.56 varies by ±0.1 for different degrees of dispersion. When the transport is highly dispersive, the capacitance is larger than C_{geo} at all frequencies. Consequently, τ_r cannot be resolved. An example is shown in the bottom panel of Fig. 1, curve (c). Below, we demonstrate that AS, along with the computer-simulated $-\Delta B$, can be used to extract the mobility of an organic charge transporter.

III. EXPERIMENT

The samples used in this study had a general structure of anode/m-MTDATA/cathode. m-MTDATA was obtained from Syntec GmbH. It was used without further purification. The chemical structure of m-MTDATA is shown in the inset of Fig. 3. The thicknesses of the organic films were measured by a profilometer (Tencor, Alpha-step 500). Prepatterned indium tin oxide (ITO) on glass was used as the anode. The ITO substrate was cleaned by a sequence of ultrasonic baths and by uv-ozone treatment.

For TOF measurements, a thick (3.5 μm) film of m-MTDATA was thermally evaporated onto ITO in vacuum with a base pressure of 10^{-6} Torr. A semitransparent aluminum (Al) film was subsequently evaporated onto m-MTDATA to form the cathode. Details of TOF experimental setup were described elsewhere.[14] The m-MTDATA film was photoexcited through the Al side by a nitrogen pulsed laser ($\lambda=337$ nm and pulse width=4 ns). The laser power was adjusted to avoid space charge effect. A dc power supply was used to provide an external voltage bias to extract the photogenerated holes. The photocurrent transient was finally monitored by a digital oscilloscope (HP54600B) through a sensing resistor in series with the sample.

For current-voltage and admittance measurements, ITO or gold (Au) was used as the anode. A thinner layer (735 nm) of m-MTDATA was coated on the anode. Ag was then evaporated on m-MTDATA to form the cathode. The Ag cathode also acts as an electron-blocking contact. Since there is a significant energy difference between the lowest unoccupied molecular orbital (LUMO) of m-MTDATA (2.0 eV) and the work function of Ag (4.3 eV), few electrons can be injected from the cathode. On the other hand, the ITO/m-MTDATA interface is approximately Ohmic as there is a relatively small energy difference between the work function of ITO and highest occupied molecular orbital (HOMO) of m-MTDATA.[15] Therefore the overall current is dominated by the hole current. The active area of the devices was about 0.036 cm^2. The admittance of the device was measured by an impedance analyzer (GenRad 1693 RLC Digitbridge™) as a function of frequency. To achieve this, an ac modulation of amplitude 50 mV ($f=10^2-10^5$ Hz) was superimposed on the dc-biased voltage which typically varied from 2 to 12 V. Current-voltage measurements were carried out with a source measure unit (KEITHLEY 236). During all measurements (TOF, current-voltage, and admittance), the devices were placed on a cold finger inside a cryostat (Oxford) under a pressure of 10^{-3} Torr.

IV. RESULTS AND DISCUSSION

Figure 3 shows a typical hole TOF transient at 289 K. The sample had a structure ITO/m-MTDATA (3.5 μm)/Al. The applied electric field was $E=6.27\times10^5$ V/cm. The average hole transit time τ_{dc} can be estimated from the TOF

07 January 2026 12:25:54

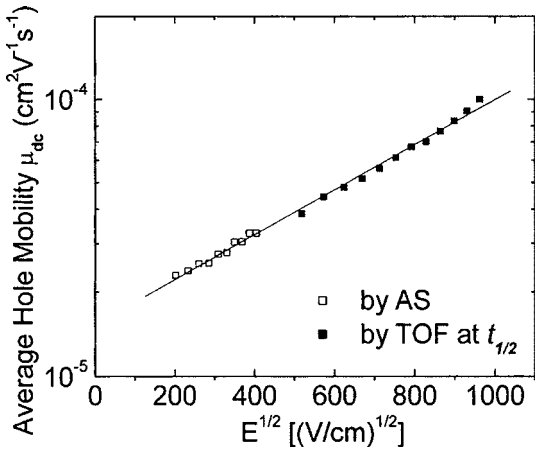

FIG. 4. Average hole mobility μ_{dc} at 289 K extracted by AS (open symbols) and by TOF at $t_{1/2}$ (filled symbols).

transient as the time $t_{1/2}$, that the current dropped to half of its value in the plateau region. From TOF results, the hole mobility μ_h can be evaluated from the relation $\mu_h = d/(t_{1/2}E)$. Figure 4, solid symbols, is a plot of μ_h vs $\sqrt{E}$. Clearly, μ_h follows the Poole-Frenkel form,

$$\mu_h = \mu_0 \exp(\beta\sqrt{E}), \tag{7}$$

where $\mu_0 = 1.3\times10^{-5}$ cm^2 V^{-1} s^{-1} and $\beta = 2.0\times10^{-3}$ $(V/cm)^{-1/2}$. Figure 5 shows the measured current-voltage (J-V) characteristics with a structure ITO/m-MTDATA (735 nm)/Ag. As indicated by the TOF transient in Fig. 3, hole transport in m-MTDATA is nondispersive. So it should exhibit trap-free space-charge-limited hole conduction (TFSCLC). Its J-V characteristics should follow the Child's law, [Appendix, Eq. (A3)]. The solid line in Fig. 4 is a fit of the Child's law to the J-V data. Clearly, the measured J-V data are in good agreement with the Child's Law. The fit also indicates that the contact between ITO and m-MTDATA is approximately Ohmic. Similar results were obtained when Au was used as the anode.

Next, we demonstrate that AS can be used all by itself to determine the hole mobility. Figure 6 shows the frequency-dependent conductance and capacitance of the same device

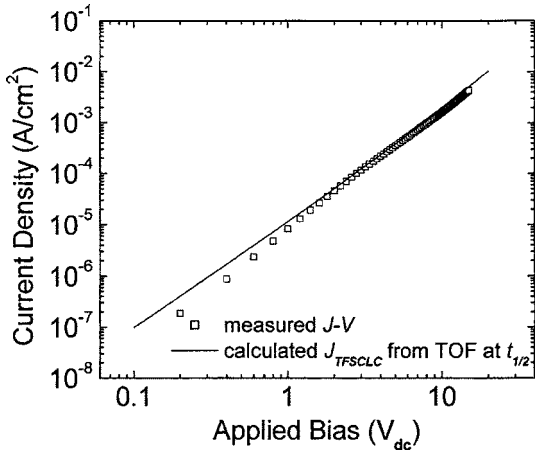

FIG. 5. J-V characteristics of ITO/m-MTDATA (735 nm)/Ag. The symbols are the experimental data. The solid line is computed from the TFSCLC theory.

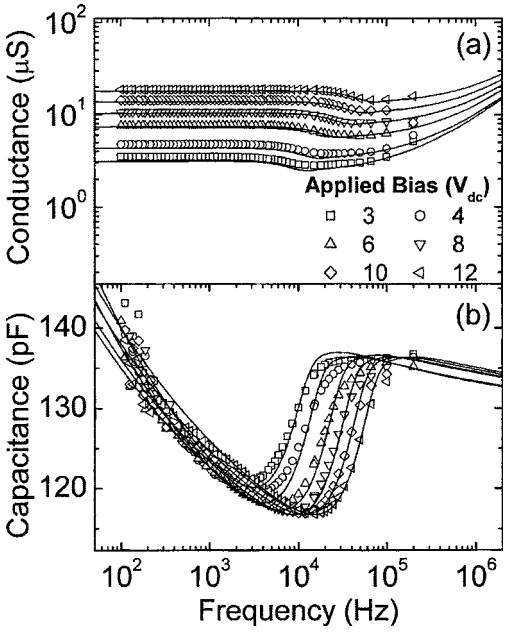

FIG. 6. Conductance (upper) and capacitance (lower) of ITO/m-MTDATA (735 nm)/Ag at different applied voltages. The solid lines are fits to the data using Eqs. (5) and (6).

for J-V measurement at different V_{dc}. When a positive bias ($V_{dc} \geqslant 2$ V) is applied on the ITO anode, holes are injected into m-MTDATA and TFSCLC occurs. Figure 6(a) (top panel) shows the measured conductance G (open symbols) versus frequency f for different V_{dc}. Clearly, G increases steadily as V_{dc} increases due to increasing amount of injected holes. Figure 6(b) (bottom panel) shows the measured capacitance C versus f for different V_{dc}. At a fixed V_{dc}, C goes through a minimum at an intermediate frequency; at high f, C reaches a steady value of about 130 pF, which is the same value as the geometric capacitance $C_{geo} = \varepsilon A/d$. The frequency-dependent G and C can be fitted by computer simulation using Eqs. (5) and (6). The results of the simulation are shown as solid lines in Fig. 6. The simulated values of G and C are in excellent agreement with the experimentally determined values. The dispersion parameters used for simulations are $M = 0.070\pm0.005$ and $\alpha = 0.18\pm0.02$ for V_{dc} between 3 and 12 V. The small value of M suggests that hole transport in m-MTDATA is essentially "trap-free" and nondispersive.

In order to extract carrier mobilities from the admittance data, the experimental negative differential susceptance $-\Delta B = -\omega(C - C_{geo})$ is plotted versus f in Fig. 7. The open symbols are the experimental data whereas the simulated results are shown in solid lines. For each set of data, a maximum in the $-\Delta B$ plot occurs. This maximum shifts to higher frequency as V_{dc} increases. The location of the relaxation peak τ_r^{-1} for each V_{dc} can be clearly resolved. Knowing τ_r, we apply the relation $\tau_{dc} = 0.56\tau_r$ to evaluate the average hole transit time τ_{dc} and therefore the average hole mobility μ_{dc}. The results at room temperature are summarized in Fig. 4. The open symbols are hole mobilities derived from AS. The solid symbols are hole mobilities derived from TOF. The two sets of mobility data are in excellent agreement with each other. From the admittance results, the zero-field mobility

07 January 2026 12:25:54

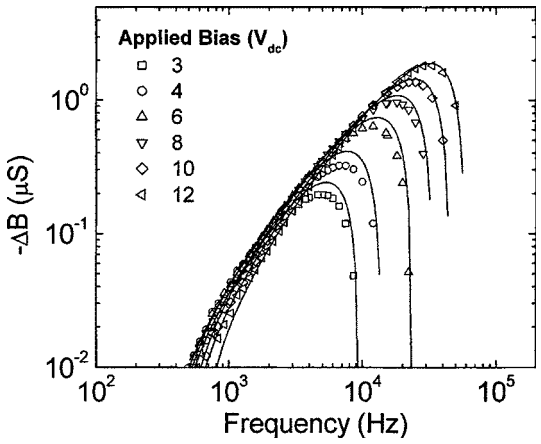

FIG. 7. Symbols: negative differential susceptances $-\Delta B$ derived from capacitance data in Fig. 6. The solid lines are simulated $-\Delta B$.

and the Poole-Frenkel slope are $\mu_0=1.5\times10^{-5}$ cm^2 V^{-1} s^{-1} and $\beta=1.9\times10^{-3}$ (V/cm)$^{-1/2}$, respectively. These values are in excellent agreement with those from independent TOF where $\mu_0=1.3\times10^{-5}$ cm^2 V^{-1} s^{-1} and $\beta=2.0\times10^{-3}$ (V/cm)$^{-1/2}$.

To further demonstrate the validity of AS, a temperature-dependent experiment was carried out. Figure 8 shows a set of temperature-dependent hole mobilities derived from AS. The data in Fig. 8 can be analyzed by the well-known GDM.[16] In the GDM, the organic material under investigation is viewed as an ensemble of transport sites for hopping conduction. Each molecule is a transport site for charge carriers. Charge conduction is thermally activated and is therefore temperature dependent. The essence of the GDM can be summarized by the semiempirical equation,

$$\mu(E,T)=\mu_{\inf}\exp\left[-\left(\frac{2\sigma}{3kT}\right)^2\right]\exp(\beta\sqrt{E}), \tag{8}$$

where

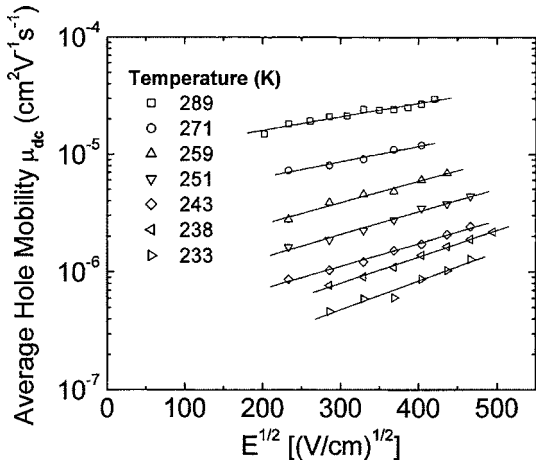

FIG. 8. The field dependent μ_{dc} extracted by AS vs the square root of the applied electric field $E^{1/2}$ at different temperatures. The solid lines are the best line fits to the data.

TABLE I. GDM disorder parameters from AS and TOF analyses.

	σ (eV)	Σ	C
AS	0.110	3.17	2.74×10^{-4}
TOF	0.112	3.32	2.30×10^{-4}

$$\beta=C\left[\left(\frac{\sigma}{kT}\right)^2-\Sigma^2\right]. \tag{9}$$

In Eqs. (8) and (9), T is the absolute temperature, k is the Boltzmann constant, $\mu_{\inf}$ is the high-temperature limit of the mobility, and C is a constant. The energetic disorder σ can be understood as the width of the Gaussian distribution of energy states for the transport sites while the positional disorder Σ can be understood as the positional/orientational disorder. According to Eqs. (8) and (9), σ can be determined from the slope in the $\mu_{0,T}$ vs $1/T^2$ plot, while Σ can be determined from the x intercept of the β vs $[\sigma/(kT)]^2$ plot. As shown in Fig. 9 and Table I, the GDM disorder parameters σ, Σ, and C are in good agreement with those independently extracted from TOF. Furthermore the values of the disorder parameters are comparable to those found in other phenylamine derivatives.[14,17–19]

Finally, we want to comment on the thickness of the sample d used for mobility evaluation in AS. Unlike TOF experiments, there is no intrinsic limitation on the value of d. In reality, one is limited by the maximum frequency (f_{max}) available in the impedance analyzer. For our analyzer, $f_{max}\approx100$ kHz. From the relation $\mu_{dc}=d^2/(\tau_{dc}V_{dc})$, we can easily deduce that $d>(0.56\mu_{dc}V_{dc}/f_{max})^{1/2}$. Using $\mu_{dc}\sim10^{-5}$ cm^2 V^{-1} s^{-1} and a typical $V_{dc}=10$ V, we require a sample thickness at least 230 nm in order to just sweep out the relaxation peak in the $-\Delta B$ vs f plot. So if the sample thickness were 230 nm, the relaxation peak would occur at about 100 kHz. Since we need to sample sufficient data points on either side of the peak, a sample of at least 2×230 or 460 nm should be used for any realistic mobility evaluation in our instrumentation. However, with the avail-

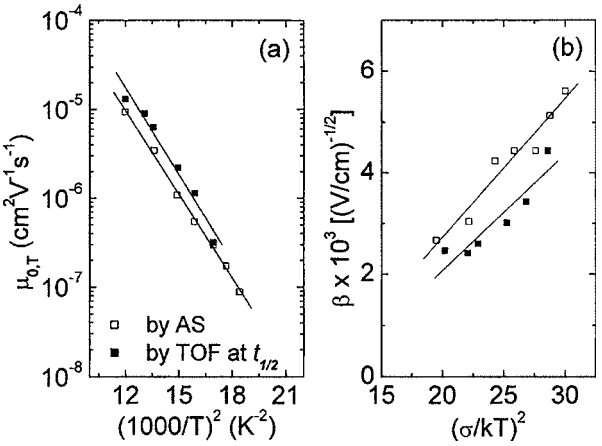

FIG. 9. (a) The zero-field mobility $\mu_{0,T}$ vs $1/T^2$ and (b) the corresponding field dependent β vs $1/T^2$. The energetic and the positional disorder parameters of m-MTDATA can be extracted from these plots. The opened (□) and closed (■) symbols represent the data obtained by AS and TOF, respectively.

07 January 2026 12:25:54

ability of fast commercial impedance analyzers, it is expected that the AS technique can be easily applied to thinner samples.

V. CONCLUSION

In summary, we have analytically and experimentally demonstrated the feasibility of admittance spectroscopy in evaluating the carrier mobility in an organic semiconductor. *m*-MTDATA is an ideal candidate for this study because it forms an Ohmic injection contact with ITO, and its hole conduction is trap-free. The average carrier mobility μ_{dc} can be extracted by AS using the position of the relaxation peak τ_r^{-1} in the negative differential susceptance plot. We found from computer simulation that the average transit time τ_{dc} is related to τ_r by $\tau_{dc}=(0.56\pm0.1)\tau_r$ for different degrees of dispersion. Hole mobilities of *m*-MTDATA determined from AS are in excellent agreement with those from an independent TOF experiment. The mobilities from AS are further analyzed by the GDM. The positional and energetic disorder parameters determined by AS and TOF are also in good agreement. Admittance spectroscopy appears to be a very valuable tool in evaluating the carrier transport properties in organic semiconductors with the advantage of relatively little material consumption.

ACKNOWLEDGMENTS

Support of this research by the Research Committee of Hong Kong Baptist University and the Research Grant Council of Hong Kong under HKBU/211205 are gratefully acknowledged. The authors would like to thank K. L. Tong for technical solutions. One of the authors (S.W.T.) would also like to thank J. An, Professor P. Migliorato, and Dr. F. Yan for valuable discussion.

APPENDIX: DERIVATION OF THE COMPLEX ADMITTANCE OF AN ORGANIC FILM

At the anode, an Ohmic injection contact implies the boundary condition $E(0,t)=0$. In the absence of any ac perturbation, the electric field is independent of time. So, $\partial E(x,t)/\partial t=0$. Combining Eqs. (1) and (2), we can write the dc electric field and the hole density as[20]

$$E_{dc}(x)=\sqrt{\frac{2J}{\varepsilon\mu_{dc}}}x^{1/2}, \tag{A1}$$

$$\rho_{dc}(x)=\frac{\varepsilon}{2q}\sqrt{\frac{2J}{\varepsilon\mu_{dc}}}x^{-1/2}. \tag{A2}$$

The current density (J)-voltage (V) characteristics can be described by Child's law,

$$J_{TFSCLC}=\frac{9}{8}\mu_{dc}\varepsilon\frac{V^2}{d^3}. \tag{A3}$$

Equations (A1) and (A2) can be rewritten using Eq. (A3) and the relation $\mu_{dc}=d^2/\tau_{dc}V_{dc}$, where τ_{dc} is the average carrier transit time. The dc electric field and the hole density become

$$E_{dc}(x)=\frac{3\sqrt{d}}{2\tau_{dc}\mu_{dc}}x^{1/2}, \tag{A4}$$

$$\rho_{dc}(x)=\frac{3\varepsilon\sqrt{d}}{4q\tau_{dc}\mu_{dc}}x^{-1/2}. \tag{A5}$$

Next, we analyze the solution to the Poisson equation and the current density when a small ac signal v_{ac} is superimposed on V_{dc}. The solutions to Eqs. (1) and (2) can be written as the sum of dc and time-dependent contributions $e(x,t)$, $\vartheta(x,t)$, and $j(t)$ to the electric field, charge density, and current density, respectively,

$$\begin{aligned} E(x,t)&=E_{dc}(x)+e(x,t),\\ \rho(x,t)&=\rho_{dc}(x)+\vartheta(x,t),\\ J(t)&=J_{dc}+j(t). \end{aligned} \tag{A6}$$

The resulting first-order small signal time-dependent current density becomes

$$j(t)=q\mu(t)\rho_{dc}e(x,t)+\varepsilon\mu(t)E_{dc}\frac{\partial e(x,t)}{\partial x}+\varepsilon\frac{\partial e(x,t)}{\partial t}. \tag{A7}$$

The first term on the right-hand side of Eq. (A7) describes the response of the dc charge density to the ac field. The second term gives the current due to the additional time-dependent injected charge-carrier density. The last term is due to the displacement current by carrier relaxation. Since the admittance $Y\equiv i_{ac}/v_{ac}$, where $i_{ac}=Aj$, the ac electric field $e(x,t)$ in Eq. (A7) should be solved. Applying Fourier transform to Eq. (A7), one obtains

$$j(\omega)=q\mu(\omega)\rho_{dc}e(x,\omega)+\varepsilon\mu(\omega)E_{dc}\frac{\partial e(x,\omega)}{\partial x}+i\omega\varepsilon e(x,\omega). \tag{A8}$$

E_{dc} and ρ_{dc} in Eq. (A8) can be eliminated using Eqs. (A4) and (A5), giving

$$\begin{aligned} j(\omega)=&\frac{3\varepsilon\sqrt{d}\tilde{\mu}(\omega)}{4\tau_{dc}}x^{-1/2}e(x,\omega)+\frac{3\varepsilon\sqrt{d}\tilde{\mu}(\omega)}{2\tau_{dc}}x^{1/2}\frac{\partial e(x,\omega)}{\partial x}\\ &+i\omega\varepsilon e(x,\omega), \end{aligned} \tag{A9}$$

where $\tilde{\mu}(\omega)=\mu(\omega)/\mu_{dc}$ is defined as the normalized mobility. Equation (A9) is a first-order differential equation with respect to $e(x,\omega)$. The solution is

$$\begin{aligned} e(x,\omega)=\frac{j(\omega)}{i\omega\varepsilon}\Bigg(1-&\frac{3\sqrt{d}\tilde{\mu}(\omega)}{4i\omega\tau_{dc}}x^{-1/2}\\ &\times\left\{1-\exp\left[\frac{-i4\omega\tau_{dc}}{3\sqrt{d}\tilde{\mu}(\omega)}x^{1/2}\right]\right\}\Bigg). \end{aligned} \tag{A10}$$

Since $v_{ac}(\omega)=\int_0^d e(x,\omega)dx$, we find that

07 January 2026 12:25:54

$$\nu_{ac}(\omega) = \frac{j(\omega)}{i\omega\varepsilon}\left(d - \frac{3d\tilde{\mu}(\omega)}{2i\omega\tau_{dc}} - 2d\left[\frac{3\tilde{\mu}(\omega)}{4\omega\tau_{dc}}\right]^2 \times\left\{1 - \exp\left[\frac{-i4\omega\tau_{dc}}{3\tilde{\mu}(\omega)}\right]\right\}\right). \quad \text{(A11)}$$

We define the normalized frequency as $\Omega = \omega\tau_{dc}$. Equation (A11) can be written as

$$\nu_{ac}(\Omega) = \frac{j(\Omega)\tau_{dc}d}{\Omega^3\varepsilon}\left(-i\Omega^2 + 1.5\tilde{\mu}(\Omega)\Omega + 2i[0.75\tilde{\mu}(\Omega)]^2\left\{1 - \exp\left[\frac{-i4\Omega}{3\tilde{\mu}(\Omega)}\right]\right\}\right). \quad \text{(A12)}$$

As $Y(\Omega) = i_{ac}/\nu_{ac}$, and recall $i_{ac} = Aj$, one can rearrange (A12) to give

$$Y(\Omega) = \frac{\varepsilon A}{\tau_{dc}d}\left(\frac{\Omega^3}{2i[0.75\tilde{\mu}(\Omega)]^2\{1 - \exp[-i4\Omega/3\tilde{\mu}(\Omega)]\} + 1.5\tilde{\mu}(\Omega)\Omega - i\Omega^2}\right). \quad \text{(A13)}$$

Equation (A13) describes the frequency-dependent electrical response of the carriers inside the organic film.

[1] C. W. Tang and S. A. VanSlyke, Appl. Phys. Lett. **51**, 931 (1987).
[2] F. De Angelis, S. Cipolloni, L. Mariucci, and G. Fortunato, Appl. Phys. Lett. **86**, 203505 (2005).
[3] N. J. Haddock, B. Domercq, and B. Kippelen, Electron. Lett. **41**, 444 (2005).
[4] J. Xue, S. Uchida, B. P. Rand, and S. R. Forrest, Appl. Phys. Lett. **84**, 3013 (2004).
[5] S. Yoo, B. Domercq, and B. Kippelen, Appl. Phys. Lett. **85**, 5427 (2004).
[6] P. W. M. Blom and M. C. J. M. Vissenberg, Mater. Sci. Eng., R. **27**, 53 (2000); Y. Shen, A. R. Hosseini, M. H. Wong, and G. G. Malliaras, ChemPhysChem **5**, 16 (2004).
[7] P. M. Borsenberger and D. S. Weiss, *Organic Photoreceptors for Imaging Systems* (Marcel Dekker, New York, 1993), Chap. 9.
[8] H. C. F. Martens, H. B. Brom, and P. W. M. Blom, Phys. Rev. B **60**, R8489 (1999).
[9] S. Berleb and W. Brütting, Phys. Rev. Lett. **89**, 286601 (2002).
[10] H. H. P. Gommans, M. Kemerink, G. G. Andersson, and R. M. T. Pijper, Phys. Rev. B **69**, 155216 (2004).
[11] H. Böttger and V. V. Bryksin, *Hopping Conduction in Solids* (Akademie-Verlag, Berlin, 1985), Chap. 6, p. 224.
[12] H. C. F. Martens, J. N. Huiberts, and P. W. M. Blom, Appl. Phys. Lett. **77**, 1852 (2000).
[13] H. C. F. Martens, W. F. Pasveer, H. B. Brom, J. N. Huiberts, and P. W. M. Blom, Phys. Rev. B **63**, 125328 (2001).
[14] H. H. Fong, K. C. Lun, and S. K. So, Chem. Phys. Lett. **353**, 407 (2002); S. C. Tse, H. H. Fong, and S. K. So, J. Appl. Phys. **94**, 2033 (2003).
[15] C. Giebeler, H. Antoniadis, D. D. C. Bradley, and Y. Shirota, Appl. Phys. Lett. **72**, 2448 (1998).
[16] H. Bässler, Phys. Status Solidi B **175**, 15 (1993).
[17] S. Heun and P. M. Borsenberger, Chem. Phys. **200**, 245 (1995).
[18] M. Stolka, J. F. Yanus, and D. M. Pai, J. Phys. Chem. **88**, 4707 (1984).
[19] J. Staudigel, M. Stössel, F. Steuber, and J. Simmerer, Appl. Phys. Lett. **75**, 217 (1999).
[20] M. A. Lampert and P. Mark, *Current Injection in Solids* (Academic, New York, 1970).

07 January 2026 12:25:54